Confined few-particle systems beyond mean-field theory adopting Gaussian-type orbitals and Morse interparticle interaction

Matee ur Rehman [1,*] Paul Winter [1,†] Fabio Revuelta [2] and Alejandro Saenz [1]

[1]*AG Moderne Optik, Institut für Physik, Humboldt-Universität zu Berlin, Newtonstr. 15, D-12 489 Berlin, Germany*

[2]*Grupo de Sistemas Complejos, Escuela Técnica Superior de Ingeniería Agronómica, Alimentaria y de Biosistemas, Universidad Politécnica de Madrid, Avenida Puerta de Hierro 2-4, 28040 Madrid, Spain*

(Received 15 September 2025; accepted 25 November 2025; published 22 December 2025)

Recent advancements in optical tweezers enable the trapping of arbitrary numbers of neutral atoms and molecules, and even arrays of tweezers with variable geometry can be realized. These fascinating breakthroughs require novel full-dimensional beyond mean-field treatments for systems with more than two confined particles spread over traps that are arranged arbitrarily in space. In this work, the suitability of a quantum-chemistry inspired approach adopting Cartesian Gaussians as basis functions is investigated. For this purpose, the six-dimensional integrals associated with a realistic atom-atom interaction described by a Morse model potential were implemented. The performance, correctness, and efficiency of the implementation is assessed by comparing full configuration-interaction calculations (exact diagonalizations) for two atoms in an isotropic harmonic trap with quasiexact reference results.

DOI: 10.1103/pf98-jls2

I. INTRODUCTION

The experimental development of depositing single atoms into optical tweezer arrays of in principle arbitrary shape has emerged as a powerful platform for quantum simulation and computation [1–3], quantum information processing [4], and high-precision atomic clocks [5]. This fascinating tool has now been expanded with the development of trapping molecules [6,7], thanks to the exquisite degree of control of the interparticle interaction via magnetic Feshbach resonances [8,9]. Remarkably, it became possible to move tweezers or tweezer arrays relative to each other [10], allowing also for merging them, e.g., in order to replicate molecular configurations out of individual atoms [11,12].

All these novel experiment setups require proper theoretical and numerical descriptions which are, nonetheless, extraordinarily challenging. The computational demands become particularly high under three-dimensional confinements [13,14], especially for complex trapping geometries without symmetry, as, then, dimensionality reduction [15–17] becomes unfeasible. The situation is even more involved when the trap dimension is similar to the effective atom-atom interaction length, because the trap and the interparticle interaction potentials need to be treated simultaneously and on a comparable level of accuracy. Within this regime, novel phenomena like the so-called inelastic confinement-induced resonances [14,18–21] may appear, which may be used for the coherent formation of molecules [22,23] or become a noticeable nuisance in quantum-simulation experiments, especially if their occurrence is unknown. The influence of the confining potentials of a tweezer array on, e.g., exotic bound states like the Efimov trimers [24–31] is another problem of current interest.

Due to the short-range interaction between two ultracold atoms, a second approximation that is routinely adopted concerns the use of pseudopotentials, which are computationally less demanding than realistic particle-particle interactions [13]. Remarkably, these models accurately describe the wave functions at long range despite not reproducing correctly the true shape of the physical (short-range) particle-particle interaction. The popularity of the pseudopotentials is based on their remarkable ability to greatly simplify the six-dimensional two-particle integrals that appear in the full three-dimensional treatment of two or more particles. (The integrals are even higher dimensional if geminals, i.e., two-particle basis functions, are adopted.) Moreover, the number of these integrals increases with the fourth power of the number of single-particle basis functions in a naive approach. Despite numerous tricks, the number of integrals still scales exponentially.

Harmonic [32] and Gaussian [30,33–35] pseudopotentials are widely spread as they render two-particle integrals that can be computed straightforwardly if, e.g., (Cartesian) Gaussian basis functions [36] or Gaussian geminals [37,38] are used. However, the most popular approximation within the ultracold community is, by far, the (regularized) δ contactlike function. Undoubtedly, this leads to a drastic simplification of the two-particle integrals, reducing the dimension from 6 to 3. However, under three-dimensional confinement the (regularized) δ-function pseudopotential fails to converge

*Contact author: rehmanmatee@physik.hu-berlin.de

†Present address: Institut für Theoretische Physik, Leibniz Universität Hannover, Appelstraße 2, 30167 Hannover, Germany.

Published by the American Physical Society under the terms of the Creative Commons Attribution 4.0 International license. Further distribution of this work must maintain attribution to the author(s) and the published article's title, journal citation, and DOI.

in beyond-mean-field approaches like exact diagonalization [39]. Therefore, a renormalization is required (see Ref. [40] and references therein), which, in turn, massively complicates the treatment [41].

All the previous approaches have been extremely fruitful. Unfortunately, they cannot be straightforwardly applied to the much more intriguing experimental situations, where the full dimensionality of the system must be taken into account and a detailed description of the interparticle potential is required, such as those provided by optical tweezer arrays arranged in complex geometries or strictly three-dimensional optical lattices. These setups closely resemble those in electronic-structure calculations [42], where the interacting ultracold atoms (or molecules) explore the optical traps in a similar fashion as the electrons (within the Born-Oppenheimer approximation) sojourn the potential energy surfaces. Thus, it appears natural to implement a quantum-chemistry perspective to this atomic problem in order to benefit from the impressive efficiency of the various numerical packages developed over time.

Most of the quantum-chemistry approaches adopt Gaussian basis functions, here called Gaussian-type orbitals (GTOs). However, Gaussians neither possess the proper shape close to the nuclei nor at large distances, but the occurring six-dimensional integrals can be much more efficiently solved than in the case of hydrogenic basis functions (Slater-type orbitals). In the case of ultracold atoms, GTOs placed at the centers of the various potential wells of the tweezer array (and in between, for higher precision) provide very flexible and suitable basis-function sets. Moreover, these functions are very suitable as the wells, in first-order approximation, are harmonic. Notice, however, that sets of perfectly harmonic (or polynomial) potentials are not suitable, as they lead to nonphysical infinitely high potential barriers.

However, transferring electronic-structure methods to ultracold atomic systems is far from straightforward. In contrast to the case of only spin-1/2 electrons, ultracold atomic ensembles can comprise a wide variety of constituents, ranging from Fermions with spin numbers different from 1/2 to Bosons with integer spins, and mixtures thereof. More importantly, the (effective) interaction potential between two ultracold atoms is typically known only from molecular Born–Oppenheimer calculations, spectroscopic data, or a combination of both, and they are, in general, only numerically provided. These interaction potentials depend on the specific atomic pair under consideration and are considerably more complex than the analytically defined Coulombic repulsion between electrons. Furthermore, they exhibit an attractive region at intermediate interatomic separations, supporting numerous molecular (diatomic) bound states.

A central question is, therefore, whether the vast number of two-particle integrals often involving up to four distinct, potentially multicentered GTOs can be computed with sufficient accuracy and efficiency for realistic interatomic potentials. This challenge arises because the sophisticated algorithms developed for the efficient evaluation of purely Coulombic interactions, which form the backbone of electronic-structure codes, cannot be directly or, in some cases, at all applied to these more general interaction forms. This applies especially in regimens where the (effective) interatomic interaction, either attractive or repulsive, becomes comparable in strength to the trapping potential.

In contrast to most quantum-chemistry calculations that concentrate on the electronic ground state or possibly some low-lying excited states, in the case of trapped ultracold atoms the interest often involves a series of states, e.g., in studies of inelastic confinement-induced resonances [14,18,23]. Similarly, investigating relaxation dynamics and thermalization in many-body quantum systems necessitates the computation of excited eigenfunctions. The behavior of these systems can vary significantly depending on whether the eigenfunction thermalization hypothesis is satisfied [43–45]. Notably, deviations from the previous hypothesis such as those arising from quantum many-body scarring [46–48] lead to atypical dynamical behavior. Eigenfunctions of excited states are also central to the phenomenon of single-particle scarring, which is crucial for understanding the unexpected localization of wave functions along unstable periodic orbits [49].

In this work, a quantum-chemistry inspired description of ultracold atoms trapped in tweezer arrays in which the potential wells are arbitrarily distributed in space is discussed. The most important ingredient, the corresponding integrals involving GTOs, has been implemented and numerically tested. Within the approach, Cartesian or spherical Gaussians, preferentially but not necessarily positioned at the centers of the tweezer potential wells, are adopted as single-particle basis functions. Many-particle wave functions are expressed as linear combinations of properly symmetrized (Bosonic atoms) or antisymmetrized (Fermionic atoms) one-particle tensor-product states (configurations). As in electronic-structure calculations, the configurations may be formed adopting one-particle wave functions from a mean-field (or density-functional) calculation. Different choices of the configurations adopted in solving the many-particle problem like, e.g., full or singles-doubles (multireference) configuration interaction (CI) or coupled-cluster approaches (see, e.g., Ref. [50] and references therein), allow for compromising between the required computational resources and the precision that can be achieved. While approaches adopting explicitly correlated basis functions (geminals) are known to be much more efficient in coping with correlation, they tend to become quickly intractable for an increasing number of particles. Most importantly, the problem of implementing realistic interaction potentials for geminals would need to be solved. Also approaches such as the multiconfiguration time-dependent Hartree method for Bosons [51] employ a pseudopotential approximation for the interparticle interaction.

Alternatively, the Jacobi coordinates are adopted, see, e.g., Refs. [52–55]. However, the number of coordinates and thus the computational efforts increase drastically with the number of particles. Furthermore, the incorporation of multicentered trap potentials appears nontrivial. Similarly, so far the use of hyperspherical coordinates, see, e.g., Refs. [56–58], seems to be limited to at most isotropic (harmonic) trap potentials or to reduced dimensions. Therefore, an extension to the multicenter case appears to be very challenging and far from being straightforward.

In order to overcome these limitations, a GTO-based approach is introduced in this work. This approach is very flexible and allows for different levels of approximation

ranging from mean field over density-functional theory to (multireference) CI, coupled cluster, or full-CI quantum Monte Carlo. The present method builds upon Refs. [59,60], which demonstrated that the six-dimensional two-particle integrals involving products of up to four distinct (possibly multicentered) GTOs and an isotropic function of the relative coordinate can be reformulated as a multiple sum over one-dimensional master integrals.

As a proof of concept, and before tackling the more ambitious goal of studying many interacting ultracold atoms (or molecules) trapped in multicentered optical tweezer arrays with arbitrarily distributed potential wells, we focus here on a simpler system consisting of two indistinguishable Bosonic atoms confined in a harmonic trap, with their interatomic interaction described by a realistic Morse potential. For this system, quasiexact reference data can be obtained (see, e.g., Ref. [61]), enabling a stringent validation of both the correctness of our implementation and the convergence behavior of GTO-based representations. GTOs optimized for single-well potentials are expected to provide a reliable foundation for future multiwell studies. This parallels standard quantum-chemistry practice, where atomic GTOs serve as initial basis functions in molecular calculations or as starting points for further optimization.

The remaining of this paper is organized as follows. Section II introduces the method with a particular emphasis on the evaluation of the two-particle integrals for the Morse interaction potential considered in this work. Section III presents and discusses the results, i.e., basis-set convergence and a comparison of the energy spectrum and eigenfunctions with reference data. Finally, in Sec. IV, an outlook and a discussion on the future research directions and applications is provided.

II. METHOD

A. Configuration-interaction with Gaussians

The stationary Schrödinger equation in absolute coordinates for N identical particles trapped in a three-dimensional potential is

$$\left[\sum_{i=1}^{N}\left(-\frac{\hbar^2}{2m_{\rm i}}\nabla^2_{\mathbf{r}_i}+\hat{\rm V}_{{\rm trap},i}(\mathbf{r}_i)+\sum_{j>i}^{N}\hat{\rm U}(r_{ij})\right)\right]\Psi = E\,\Psi, \tag{1}$$

where $\Psi=\Psi(\mathbf{r}_1,\ldots,\mathbf{r}_N)$ is the wave function for the N particles. The first term in the sum is the kinetic-energy operator of the ith particle and $\hat{\rm V}_{{\rm trap},i}(\mathbf{r}_i)$ is the external (tweezer-array) trapping potential. Finally, $\hat{\rm U}(r_{ij})$ is the interatomic-interaction potential that is assumed to be isotropic and thus to depend solely on the interatomic distance $r_{ij}=|\mathbf{r}_i-\mathbf{r}_j|$.

Within the CI ansatz [62], also known as exact diagonalization, the wave function Ψ is expressed as a linear combination of $N_{\rm CF}$ configurations Φ

$$\Psi(\mathbf{r}_1,\ldots,\mathbf{r}_N)=\sum_{j=1}^{N_{\rm CF}} c_j\,\Phi_j(\mathbf{r}_1,\ldots,\mathbf{r}_N). \tag{2}$$

These configurations,

$$\Phi_j(\mathbf{r}_1,\ldots,\mathbf{r}_N)=\hat{\rm S}_N^{(\pm)}\prod_{\tau=1}^{N}\phi_\tau(\mathbf{r}_\tau), \tag{3}$$

are (anti-)symmetrized $(-/+)$ products of one-particle wave functions ϕ, where $\hat{\rm S}_N^{(\pm)}$ is the (anti-)symmetrization operator, which may include an appropriate normalization factor. If all configurations Φ that can be constructed from a given set of one-particle wave functions are included, the approach is known as full CI. Full CI calculations are computationally extremely expensive and, in practice, restricted to a very small number of particles and one-particle wave functions. Therefore, most of the CI calculations include only a (very) limited number of configurations instead of the complete set. In order to still obtain good results, both the selection of the configurations Φ as well as the quality of the adopted one-particle wave functions ϕ is of crucial importance.

The traditionally most common choice consists in building a reference configuration from the mean-field (Hartree-Fock) orbitals that are occupied in the ground state. Then, all the configurations that can be obtained by transferring one (or two) electron(s) from the reference configuration to an unoccupied orbital are added. This is known as CI singles (or CI singles and doubles). The optimization of the choice of configurations remains an active subject of investigation [63]. Examples are restricted and complete active space (RAS or CAS) CI [64], multireference configuration interaction (MRCI) [65], or full-CI quantum Monte Carlo (FCIQMC) approaches [66,67]. A size-consistent selection of configurations is provided by coupled-cluster methods [50]. Comparable accuracy can be achieved with much fewer configurations if the orbitals are simultaneously varied as in multiconfiguration self-consistent-field approaches (MCSCF) [68], including again restricted or complete active spaces (RASSCF or CASSCF) [69–71]. Common to all these approaches is the use of single-particle basis functions and the key ingredient of corresponding structure codes is the solution of the six-dimensional particle-particle interaction integrals. The efficient evaluation in the case of the most frequently adopted GTOs, but for a realistic interatomic interaction potential instead of the bare Coulombic interaction encountered in electronic-structure calculations, is the central part of this work. For the simple two-particle example considered in this exploratory work, full CI is adopted. Since the mean-field orbitals and the basis functions are related by a unitary transformation, identical results are obtained in a full CI if the configurations are either built from mean-field orbitals or directly from the basis functions. Thus, no mean-field orbitals are calculated in this work.

Usually, multicenter integrals involving GTOs are most suitably calculated in Cartesian coordinates. Therefore, Cartesian GTOs, defined as

$$\phi_\tau(\mathbf{r})=\mathcal{N}_\tau(x-A_x)^i\,(y-A_y)^k\,(z-A_z)^m e^{-\tau(\mathbf{r}-\mathbf{A})^2}, \tag{4}$$

are often adopted in quantum-chemistry calculations. They are, thus, characterized by the set of parameters i,k,m,τ, and $\mathbf{A}$, with $i,k,m\in\mathbb{N}_0$, the width of the orbital $\tau\in\mathbb{R}^+$, the center of the Gaussian $\mathbf{A}=(A_x,A_y,A_z)\in\mathbb{R}^3$, and the

normalization factor

$$\mathcal{N}_\tau = \left(\frac{2\tau}{\pi}\right)^{\frac{3}{4}} \sqrt{\frac{(4\tau)^{i+k+m}}{(2i-1)!!(2k-1)!!(2m-1)!!}}. \quad (5)$$

The number of Cartesian Gaussians for a given value of $\sigma := i+k+m$ is $(\sigma+1)(\sigma+2)/2$. Only for $\sigma = 0$ or 1 there is (in the isotropic case) a one-to-one correspondence with the quantum number of angular momentum ℓ (see Appendix A).

In most cases, an isotropic particle-particle interaction potential commutes with all symmetry elements of the one-particle Hamiltonian. Then, the standard group-theoretical methods can be applied straightforwardly to obtain symmetry-adapted configurations from symmetry-adapted one-particle orbitals, see, e.g., Ref. [72]. The demands become particularly high in situations where atomic or molecular wave functions are delocalized across multiple sites in a tweezer array. These challenges are further amplified if the array consists of wells that are arbitrarily distributed in space and potentially vary in shape, i.e., if the wells lack the symmetric arrangement characteristic of a periodic optical lattice. Since the exploratory example considered here is spherically symmetric, in contrast to tweezer arrays that are the real goal of the developed approach, no symmetry considerations are implemented in the present calculation. Still, the obtained results automatically exhibit the proper symmetries. Therefore, as concluded from the results below, both the one-particle wave functions ϕ as well as the two-electron states Ψ possess a well-defined one-particle angular momentum ℓ or total two-particle angular momentum L, respectively.

B. Two-particle integrals

The calculation of the eigenenergies and the eigenfunctions in Eq. (1) that describe ultracold atoms in a tweezer array adopting the CI ansatz (2) requires the construction of the corresponding Hamiltonian matrix in the basis of the configurations Φ. Since these configurations are expressed as products of the single-particle functions ϕ, see Eq. (3), the matrix elements of the Hamiltonian (and the overlap) between these single-particle functions ϕ are required.

First, there are the three-dimensional one-particle integrals $\langle\phi_\tau|\hat{\mathrm{O}}|\phi_\chi\rangle$, where $\hat{\mathrm{O}}$ is the identity operator (overlap), the operator of the kinetic energy, or the one of the external potential. The kinetic-energy integrals are identical to those occurring in any electronic-structure calculation that adopts GTOs. If the potential created by the tweezer array is expressed either as a polynomial or as a superposition of Gaussians with negative prefactors, then the one-particle potential-energy integrals are basically identical to an overlap integral but between three instead of two GTOs. Again, these integrals can be very efficiently evaluated, since the product of two Cartesian Gaussians renders as a new single Cartesian Gaussian.

Second, there are the six-dimensional two-particle integrals,

$$I = \langle\phi_\tau\phi_\rho|\hat{\mathrm{U}}|\phi_\chi\phi_\epsilon\rangle = \iint \mathrm{d}\mathbf{r}_1\,\mathrm{d}\mathbf{r}_2\,\phi_\tau(\mathbf{r}_1)\phi_\rho(\mathbf{r}_2)\,U(r_{12})\,\phi_\chi(\mathbf{r}_1)\phi_\epsilon(\mathbf{r}_2), \quad (6)$$

that can involve up to four different GTOs characterized by the parameters $(i,k,m,\tau,\mathbf{A})$, $(j,l,n,\chi,\mathbf{B})$, $(i',k',m',\rho,\mathbf{C})$, and $(j',l',n',\epsilon,\mathbf{D})$; see Eq. (4). These two-particle integrals are challenging, since the GTOs are formulated in the absolute Cartesian coordinates $\mathbf{r}_1$ and $\mathbf{r}_2$ of the two particles, but the isotropic interaction potential depends on the relative coordinate $r_{12} = |\mathbf{r}_1 - \mathbf{r}_2|$. In contrast to the electronic-structure problem, the interaction potential U is not a pure Coulomb potential but should be a short-range atom-atom interaction potential in the case of ultracold atoms. Most importantly, it should once more be noted that already within a mean-field calculation a tremendous amount of two-particle integrals needs to be computed. This is even worse in the case of a CI calculation. Consequently, an efficient and sufficiently accurate evaluation of the two-particle interaction integrals is of crucial importance.

In this work, the Morse interaction potential is employed. It has a long history in the parametrization of the atom-atom interactions, i.e., of Born-Oppenheimer or spectroscopically obtained potential curves of diatomic molecules [73,74]. There are different ways to write the Morse potential with corresponding differences in the definition of its parameters. Here, the Morse potential is used in the form

$$U(r_{12}) = D_e(e^{-2a_m(r_{12}-R_m)} - 2\,e^{-a_m(r_{12}-R_m)}), \quad (7)$$

where D_e is the dissociation energy, R_m defines the location of the potential minimum, and a_m defines the width of the potential. Despite of having only these three fit parameters, the Morse potential usually provides very good fits for almost all electronic bound states of diatomic molecules, especially for their electronic ground states. Furthermore, if inserted into the time-independent Schrödinger equation describing the nuclear motion of a diatomic molecule within the Born-Oppenheimer approximation, then it possesses known analytical solutions representing the rotational and vibrational degrees of freedom. In fact, the method employed here for the case of a Morse interaction potential can be rather straightforwardly extended to other atom-atom interaction model potentials like the Lennard-Jones potential [75] or even numerically provided (for example Born-Oppenheimer) potentials, as will be described in a forthcoming work. The following Sec. II C describes the details of the methods employed to evaluate the integrals for technically interested readers.

C. Analytical solution of the integrals

A general formalism for solving integrals of the type given in Eq. (6) was introduced in the Refs. [59,60]. Thus, here, only a brief summary is provided to present the reader the general idea and notation, as well as novel results for the single center case ($Q = 0$).

1. Reduction to one-dimensional form

Applying the McMurchie-Davidson scheme [76] to the product of four Cartesian GTOs in Eq. (6) potentially located at four different centers yields a product of two Cartesian Gaussians. These Gaussians, which are related to particles 1 and 2, respectively, have the exponents $p = \tau + \chi$ and $q = \rho + \epsilon$ and are centered at the positions $\mathbf{P} = \frac{\tau\mathbf{A}+\chi\mathbf{B}}{p}$ and

$\mathbf{Q} = \frac{\rho\mathbf{C}+\epsilon\mathbf{D}}{q}$. Since the integration has to be performed over the complete space, it is, without loss of generality, possible to shift the origin of the coordinate system to agree to the center of one of the two Gaussians, leading to $\mathbf{P} = 0$. Then, with the help of the Gauss-Hermite functions, Eq. (6) can be expressed as [60,77]

$$I = \sum_{t=0}^{i+j} E_t^{ij} \sum_{u=0}^{k+l} E_u^{kl} \sum_{v=0}^{m+n} E_v^{mn} (-1)^{t+u+v} \times \sum_{t'=0}^{i'+j'} E_{t'}^{i'j'} \sum_{u'=0}^{k'+l'} E_{u'}^{k'l'} \sum_{v'=0}^{m'+n'} E_{v'}^{m'n'} \times R^{t+t',u+u',v+v'}, \tag{8}$$

where the expansion coefficients, for instance E_t^{ij}, can be efficiently computed with the help of recursion relations satisfied by the GTOs [78]. The most demanding term in Eq. (8) is the R tensor. Following a special case of the Hobson theorem [79], and introducing $Q = |\mathbf{Q}|$, the R tensor can be expanded as [60]

$$R^{tuv} = \sum_{l=0}^{l_{\max}} \sum_{m=-l}^{l} c_i(l,m,t,u,v)\, Z_{lm}(\hat{Q}) \sum_{k=0}^{k_{\max}} d_k^{l,k_{\max}} \times Q^{l_{\max}-l-2k} \left(D_Q^{l_{\max}-k} B\right), \tag{9}$$

where $l_{\max} = t+u+v$ and $k_{\max} = \frac{1}{2}(l_{\max}-l)$. $\hat{Q}$ is a unit vector in the direction of $\mathbf{Q}$ and $D_Q = Q^{-1}\partial_Q$. The so-called inverse Schlegel coefficients $c_i(l,m,t,u,v)$ are given in, e.g., the Ref. [80], and the coefficients $d_k^{l,k_{\max}}$ are given in the Ref. [60]. Hence, for practical purposes, both kinds of coefficients can be precomputed and stored as a look-up table. Furthermore, the terms $Z_{lm}(\hat{Q})$ are the real solid spherical harmonics, and the term B is a function called the basic integral given by

$$B = \sqrt{\frac{\pi^5}{p+q}} \frac{1}{pq} \int_0^\infty \mathrm{d}r_{12}\, U(r_{12})\, r_{12} \times \left[\frac{e^{-\frac{pq}{p+q}(r_{12}-Q)^2} - e^{-\frac{pq}{p+q}(r_{12}+Q)^2}}{Q} \right]. \tag{10}$$

Most computational time is devoted to evaluate the derivatives of the basic integral, $D_Q^\nu B$, with $\nu = l_{\max}-k$, since they are needed in Eq. (9). For moderate and large values of Q, an effective recursive relation exists and is given in the Ref. [59]. For small Q, this recursion becomes numerically unstable and, following the suggestion in Ref. [59], the R tensor and the basic integral B are evaluated by expanding B in a Taylor series decoupling the derivatives from the integration in Eq. (10).

2. *Special case $Q = 0$*

Besides the $Q \neq 0$ cases discussed so far, $Q = 0$ also occurs if $\rho\mathbf{C} = -\epsilon\mathbf{D}$ (or if $\tau\mathbf{A} = -\chi\mathbf{B}$ and the coordinate system is chosen such that $\mathbf{Q} = \mathbf{0}$). The condition $Q = 0$ is especially met, if all four GTOs are centered at the same place, i.e., for $\mathbf{A} = \mathbf{B} = \mathbf{C} = \mathbf{D}$. As in the case of electronic-structure calculations, the accurate description of atoms in a tweezer array requires to adopt a number of GTOs centered at every potential well. Therefore, a large number of two-particle integrals with $Q = 0$ needs to be solved. It is thus important to consider this case explicitly. In fact, for $Q = 0$ the algorithm sketched in Sec. II C 1 for $Q \neq 0$ cannot be used in a straightforward way as Q appears in derivatives and denominators in Eq. (9). Alternatively, one way to evaluate the integrals in this case is to adopt the relations for $Q \neq 0$ and to extrapolate them to zero, which is rather straightforward. However, in view of the expected large number of integrals that fulfill $Q = 0$, a more resource-saving evaluation of these integrals has been developed and implemented together with the $Q \neq 0$ cases discussed above. In fact, in the course of the present work it turned out that the special implementation of the $Q = 0$ integrals is also important, since it increases the numerical accuracy.

To obtain a solution for $Q = 0$, we start with the Taylor series of B obtained in Ref. [59] for small values of Q [81]

$$B = 4\pi \left(\frac{\pi}{p+q}\right)^{3/2} e^{-\xi Q^2} \sum_{n=0}^{\infty} \frac{(2\xi Q)^{2n}}{(2n+1)!} \times \int_0^\infty \mathrm{d}r_{12}\, U(r_{12})\, r_{12}^{2n+2}\, e^{-\xi r_{12}^2}, \tag{11}$$

where $\xi = \frac{pq}{(p+q)}$. To solve the expression for the R tensor given by Eq. (9), the derivative of the above integral B has to be calculated. Since the derivative is with respect to Q, it needs to be applied on the Q-dependent terms in B, i.e., $D_Q^\nu B \propto D_Q^\nu (Q^{2n} e^{-\xi Q^2})$. Following repeated recursion, the νth derivative can be expanded as

$$D_Q^\nu (Q^{2n} e^{-\xi Q^2}) = \sum_{s=0}^{\min(\nu,n)} \binom{\nu}{s} (-2\xi)^{\nu-s} \frac{(2n)!!}{(2\nu-2s)!!} \times Q^{2\nu-2s} e^{-\xi Q^2}. \tag{12}$$

Thus, the terms other than the inverse Schlegel coefficients and the $d_k^{l,k_{\max}}$ coefficients in Eq. (9) can be simplified, along with the derivative of Eq. (12), as

$$\lim_{Q\to 0} \left[Z_{lm}(\hat{Q})\, Q^{l_{\max}-l-2k}\, D_Q^{l_{\max}-k} (Q^{2n} e^{-\xi Q^2}) \right] = \sqrt{\frac{2l+1}{4\pi}} \binom{\frac{l_{\max}}{2}}{n} (-2\xi)^{\frac{l_{\max}}{2}-n} (2n)!!\, \delta_{\mathrm{m}0}\delta_{\mathrm{l}0}\delta_{\mathrm{k}\,\frac{l_{\max}}{2}}, \tag{13}$$

where the Kronecker deltas δ_{ij} arise because only the coefficients of Q^0 survive. Hence, plugging Eq. (13) and the remaining terms of B in Eq. (11) into Eq. (9), and applying the Kronecker deltas, the R tensor can be written as

$$R^{tuv} = \frac{2\pi^2}{(p+q)^{\frac{3}{2}}} c_i(0,0,t,u,v)\, d_{\frac{l_{\max}}{2}}^{0,\frac{l_{\max}}{2}} \sum_{n=0}^{\frac{l_{\max}}{2}} \left\{ (-1)^{\frac{l_{\max}}{2}-n} \times \binom{\frac{l_{\max}}{2}}{n} \frac{(2\xi)^{n+\frac{l_{\max}}{2}}}{(2n+1)!!} \Pi_{2n+2}(\xi) \right\}, \tag{14}$$

which vanishes for odd values of $l_{\max} = t+u+v$. As previously mentioned, the inverse Schlegel coefficients c_i and the $d_{l_{\max}/2}^{0,l_{\max}/2}$ coefficients can be straightforwardly computed. As a consequence, the only demanding term present in Eq. (14) is

$\Pi_{2n+2}(\xi)$, which may be defined as

$$\Pi_\lambda(\xi) = \int_0^\infty \mathrm{d}r_{12}\, r_{12}^\lambda\, U(r_{12})\, e^{-\xi r_{12}^2} \tag{15}$$

with $\lambda = 2n + 2$. A further simplification of Eq. (15) strongly depends on the shape of the interaction potential $U(r_{12})$. Since the equation is one dimensional, we refer to it as the *master integral*. Considering the explicit example of the Morse interaction potential in Eq. (7) and inserting it into Eq. (15), the master integral can be written as

$$\Pi_\lambda(\xi) = D_e e^{-a_m R_m}[e^{-a_m R_m} S(\lambda, -2a_m, \xi) - 2S(\lambda, -a_m, \xi)]. \tag{16}$$

Here S is an integral that is described in the next section.

3. S integral

The S integral in its generic form is defined as

$$S(\alpha, \beta, \gamma) = \int_0^\infty \mathrm{d}x\, x^\alpha\, e^{\beta x - \gamma x^2}, \tag{17}$$

where α, β, and γ are real numbers with $\gamma > 0$. Assuming α to be a nonnegative integer, three different results are obtained depending on β,

$$S(\alpha, \beta, \gamma) = \begin{cases} \frac{\Gamma(\alpha+1)}{(2\sqrt{\gamma})^{\alpha+1}}\, \mathcal{U}\left(\frac{\alpha+1}{2}, \frac{1}{2}, \frac{\beta^2}{4\gamma}\right), & \text{if } \beta < 0, \\ \frac{\Gamma\left(\frac{\alpha+1}{2}\right)}{2\,\gamma^{\frac{\alpha+1}{2}}}, & \text{if } \beta = 0, \\ \frac{1}{2\,\gamma^{\frac{\alpha}{2}+1}}\left[\beta\,\Gamma\left(\frac{\alpha}{2}+1\right)\mathcal{M}\left(\frac{\alpha}{2}+1, \frac{3}{2}, \frac{\beta^2}{4\gamma}\right) + \sqrt{\gamma}\,\Gamma\left(\frac{\alpha+1}{2}\right)\mathcal{M}\left(\frac{\alpha+1}{2}, \frac{1}{2}, \frac{\beta^2}{4\gamma}\right)\right], & \text{if } \beta > 0. \end{cases} \tag{18}$$

Here Γ is the Gamma function, while $\mathcal{M}$ and $\mathcal{U}$ are the Kummer's and Tricomi's confluent hypergeometric functions, respectively [59]. Note that in Ref. [59] only the relation for $\beta < 0$ is explicitly given and thus it is implied that it remains valid for all values of β. This is the case for $\beta = 0$, though inserting $\beta = 0$ yields the compact result given on the second line of Eq. (18). If all GTOs are centered at the same location and the Morse potential is adopted to describe the interatomic interaction, as in the case in this work, then only $\beta < 0$ occurs. However, if the GTOs are centered at different locations, then for the Morse potential as well as in the case of other particle-particle interaction potentials like the Lennard-Jones or the Gaussian potentials (both have already been implemented, but will be reported elsewhere) $\beta > 0$ also occurs. All in all, the solution for $\beta > 0$ was derived and is already implemented for the planned future applications to tweezer arrays.

The calculations showed a high sensitivity to numerical errors in the evaluation of the basic integral B [see Eq. (10)]. Any numerical error propagates and accumulates through the computation of the sums in Eqs. (8) and (9). Since the S integral is calculated with the aid of the hypergeometric functions, cf. Eq. (18), a fast and accurate evaluation of these functions was mandatory. Moreover, introducing a representation for the inverse Schlegel coefficients $c_i(0, 0, t, u, v)$ and the $d^{0,l_{\max}/2}_{l_{\max}/2}$ coefficients for the particular case $Q = 0$ reduced the number of sums and function calls in the R tensor, cf. Eqs. (14) and (9). This reduced the computational time and improved the accuracy.

III. NUMERICAL RESULTS

As mentioned above, a system of two interacting ultracold Bosonic atoms trapped in a harmonic potential is considered, since accurate reference data can be obtained for validation of the results using the approach described in Refs. [61,72,82]. The length scale of the trap is defined in harmonic-oscillator units as $d_{\mathrm{ho}} = \sqrt{\hbar/\mu\omega}$, with the trap frequency ω and the reduced mass $\mu = \frac{m_1 m_2}{m_1+m_2}$. With no loss of generality, $\hbar = m = \omega = 1$ is chosen, since the present study is only meant as a proof of principles. The effective interaction between the atoms is characterized by the s-wave scattering length (a_s) [83], shown in Fig. 1 as a function of the Morse potential depth D_e. A detailed description of the basis sets employed in this work is presented in Appendix A, and the computational details for the scattering-length variation are provided in the Appendix B.

The next sections are organized as follows. Section III A provides a convergence study. Section III B compares the energy spectrum obtained using the GTOs basis set with

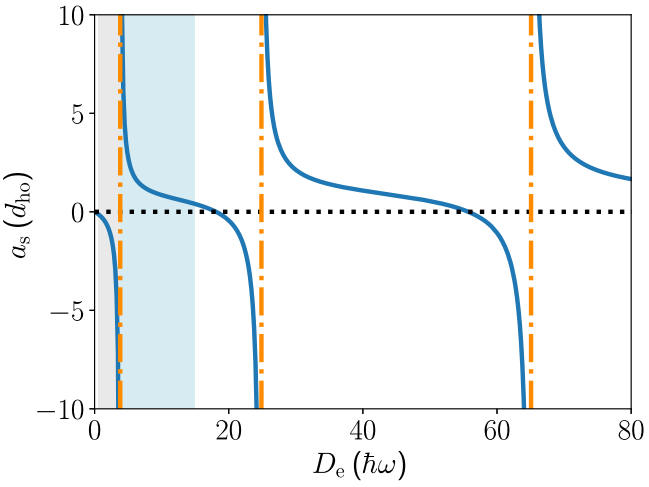


FIG. 1. Scattering length a_s (continuous blue line) of the Morse potential given by Eq. (7) for $R_m = 0.212\, d_{\mathrm{ho}}$ and $a_m = \sqrt{20}\, d_{\mathrm{ho}}^{-1}$ as a function of the potential depth D_e. The poles (vertical dashed-dotted orange) mark the positions where an additional bound state emerges as D_e increases. The gray and light blue shaded areas mark the D_e range considered in this work, where the first bound state appears in the light blue region.

reference results adopting a well-established method based on B splines and spherical harmonics. Finally, Sec. III C provides a comparative study of eigenfunctions produced by both approaches.

A. Convergence study

For a first validation of the present approach and its implementation, the convergence of the ground-state energy as a function of the number of included basis functions is investigated. Four different particle-particle-interaction strengths are considered, i.e., the Morse-potential depths $D_e = [3, 5, 10, 13]\,\hbar\omega$ that correspond to the scattering-length values $a_s = [-2.550, 2.758, 0.852, 0.579]\,d_{\mathrm{ho}}$ (cf. Fig. 1), respectively. Note that for $D_e = 3.0\,\hbar\omega$ no bound state is supported, while the remaining values chosen for D_e support a single bound state.

As previously mentioned, an efficient structure calculation requires a careful selection of the basis-set parameters. In the case of Cartesian GTOs, these parameters are the position vectors $\mathbf{A}$ of the Gaussians, the chosen types of GTOs, i.e., the values i, k, and m, and the damping exponents τ [see Eq. (4)]. The basis must be able to adequately cover the one-particle Hilbert space. Since the system considered here comprises only a single-well trap potential, GTOs centered at the origin are adopted ($\mathbf{A} = \mathbf{0}$ for all GTOs). Linear combinations of GTOs with appropriately chosen basis parameters are the eigenfunctions of the harmonic trap. Therefore, the description of noninteracting particles in a harmonic trap would be straightforward with the present approach. However, the proper description of the interaction between the atoms, especially if they form molecular bound states, is challenging when adopting trap-centered GTOs. Thus, various combinations of four different exponents τ were tested with respect to their impact on the ground-state energy. Small values of the exponents τ correspond to diffuse basis functions, while increasing values of τ lead to more localized ones.

Since even a particle-particle interaction that is isotropic with respect to the relative-motion coordinate usually breaks the single-particle symmetry, the single-particle solutions of different irreducible representations are coupled to an irreducible representation of the total system. For the case study, the ℓ and m_ℓ single-particle quantum numbers couple to the total angular momentum L (and M_L) of the two-atom system. Therefore, the addition of configurations containing orbitals with different angular momentum ℓ is needed for converged CI results, as they describe the so-called angular correlation. This applies, e.g., also to the ground state in which all particles occupy—even if the particle-particle interaction is included within the mean-field approximation—the lowest orbital which, in the present isotropic case, has $\ell = 0$ symmetry. As a consequence, the convergence behavior with respect to the exponents τ and the included types of GTOs (σ values) is not independent of each other and, in principle, the exponents τ need to be optimized whenever new GTOs are added to the calculation [see Eq. (4)]. Noticeably, the exponents τ need to be optimized separately also for each interparticle interaction and for every state if accurate results are required. In contrast, in the present exploratory study the exponents τ were optimized with the goal of finding one set of values that provides overall the lowest ground-state energies for the four scattering-length values considered. Based on a simple parameter variation, the best compromise for the GTO exponents were found to be $\tau = 0.3, 0.5, 1.0$, and 2.2.

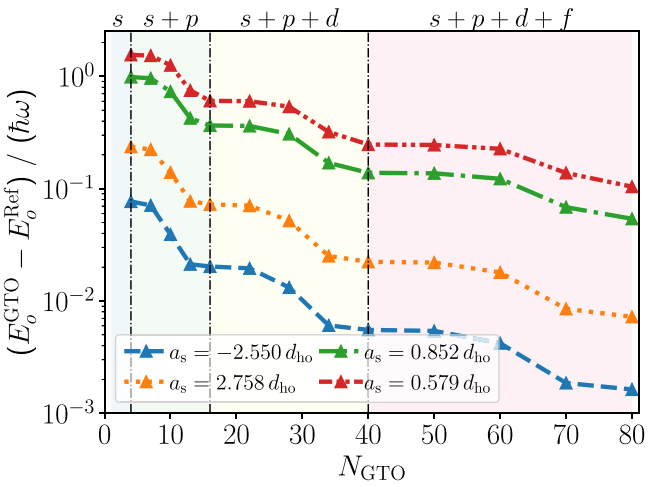


FIG. 2. The difference between the molecular ground-state energy E_0^{GTO} computed with GTOs and the corresponding reference value E_0^{Ref} as a function of the number of GTOs, N_{GTO}, for the scattering-length values given in the legend. The colored shaded areas (and the labels on the top axis) indicate the types of GTOs (s for $\sigma = 0$, p for $\sigma = 1$, d for $\sigma = 2$, and f for $\sigma = 3$) that are included.

The convergence behavior of the numerically obtained ground-state energies E_0^{GTO} as a function of the number N_{GTO} of included Cartesian GTOs is shown in Fig. 2 for the four different scattering-length values a_s. The energies are given relative to the quasiexact reference values E_0^{Ref}, i.e., $E_0^{\mathrm{GTO}} - E_0^{\mathrm{Ref}}$. Starting with a minimal basis set formed only with four s-type GTOs, the number of GTOs, N_{GTO}, is increased by adding successively four p-, d-, and f-type Cartesian GTOs, each of them comprising 3, 6, and 10 GTOs, respectively. Consistent with the variational principle, all energies E_0^{GTO} lie above the corresponding reference values E_0^{Ref} and the energy differences decrease monotonically with an increasing value of N_{GTO}.

Remarkably, the energy differences as a function of N_{GTO} of all the curves exhibit similar shapes, though some of them differ by almost two orders of magnitude. Best convergence is found for $a_s = -2.550\,d_{\mathrm{ho}}$. This is understandable, since the corresponding Morse potential with depth $D_e = 3.0\,\hbar\omega$ is not deep enough to support a molecular bound state. Therefore, the ground-state wave function is a slightly distorted trap state due to the nonzero (attractive) interatomic interaction. The second best convergence is achieved for the potential depth $D_e = 5.0\,\hbar\omega$. In this case, the ground state corresponds to a loosely bound molecular state. Therefore, the deviation from a trap state is larger than for $D_e = 3.0\,\hbar\omega$ but still comparatively small. As a consequence, the wave function is expected to be still very similar to the trap ground state. Thus, this state is well described by a relatively small number of GTOs. This changes if the particle-particle interaction increases, but still only a single molecular bound state is supported. With

increasingly attractive interaction, the bound state becomes more deeply bound and, correspondingly, the wave function becomes more compact in the relative-motion coordinate, deviating even more from the one of a trap state (see Sec. III C for details on the wave functions).

The results shown in Fig. 2 confirm the expectation that the energy convergence of the GTO basis set in absolute coordinates reduces with the depth of the interatomic interaction potential. Note that the goal of the present approach is neither the description of deeply bound molecular states nor of energetically very high-lying trap states. The former states can be efficiently treated with (standard) molecular codes, since the trap potentials are negligible. The treatment of the latter ones is also straightforward, since the interatomic interaction is negligible and thus the problem reduces, to a good approximation, to a single-particle problem.

It is interesting to note that the found convergence behavior as a function of N_{GTO} differs nevertheless almost exclusively by an overall factor (constant shift on the logarithmic scale in Fig. 2), as stated before. In fact, the optimization of the set of four τ values that provides the best overall results for all values of D_e was clearly dominated by those yielding the most deeply bound molecular ground state. As a result, the optimization of the GTO exponents τ was effectively carried out by minimizing the ground-state energy for the cases with $a_s = 0.852\, d_{\mathrm{ho}}$ and $0.579\, d_{\mathrm{ho}}$, while the results for the two other a_s values remained (automatically) well converged.

More relevant than the absolute energies are the binding energies, here defined as the difference between the corresponding noninteracting trap-state energy and the computed ground-state energy, i.e., $E_{\mathrm{binding}} = E_{\mathrm{trap}} - E_{\mathrm{computed}}$ with $E_{\mathrm{trap}} = 3\,\hbar\omega$. The relative errors (in percentages) in the binding energies obtained for 80 N_{GTO} and the four scattering-length values $a_s = [-2.550,\ 2.758,\ 0.852,\ 0.579]\, d_{\mathrm{ho}}$ are [0.315%, 0.699%, 1.811%, 2.316%], respectively.

The CPU time for one CI calculation with $N_{\mathrm{GTO}} = 80$ on a single thread of an Intel Core i9-12900K processor is 212 s and remains basically identical for the four interatomic interaction potentials considered in Fig. 2. Thus the CPU time depends basically only on the chosen basis set. The results show that the integrals, especially the ones describing the interparticle interactions adopting a realistic Morse potential, can be calculated with sufficient efficiency to allow for the theoretical treatment of few-atom systems in optical tweezer arrays, as evidently much larger basis sets are feasible than the ones used in this exploratory study. It may be noted that the number of terms in the master integral in Eq. (15), two in the case of the here considered Morse potential [see Eq. (16)], strongly affects the computational time.

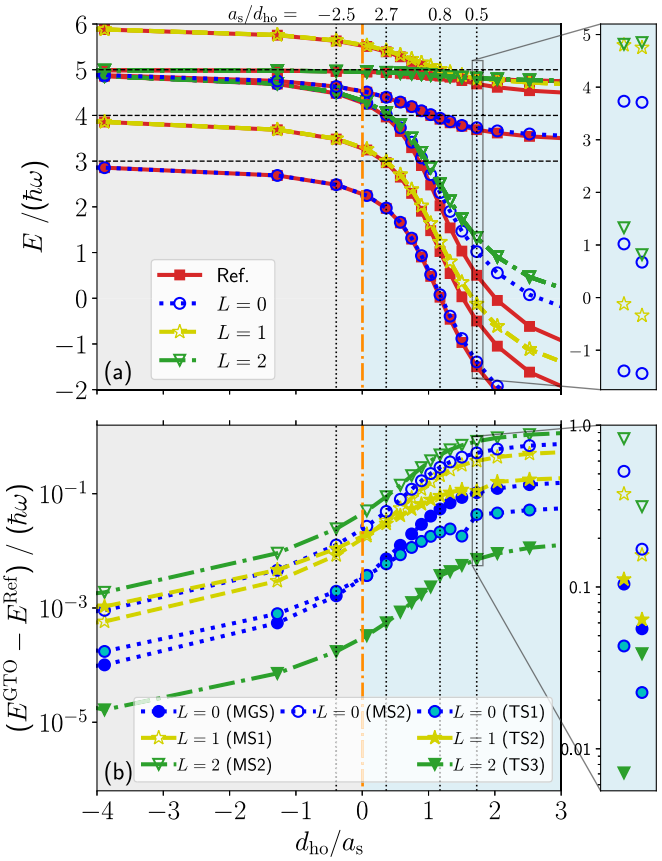


FIG. 3. (a) Energies E of some selected states of two atoms in a harmonic trap with total angular momentum L are shown as a function of the ratio between the characteristic trap size (d_{ho}) and the scattering length (a_s). The results for the GTO-1 basis set, see Appendix A, are compared to quasiexact reference results E^{Ref}. The gray and light blue shaded regions indicate the same a_s range as in Fig. 1, while the vertical orange dashed-dotted line marks the Feshbach resonance position. The dashed horizontal black lines show the asymptotic values of trap states in the absence of interatomic interaction. The vertical dotted black lines with the values of a_s/d_{ho} on the top axis correspond to the four values of a_s discussed in the convergence study in Fig. 2. (b) Deviation of the energies E^{GTO} obtained with the present GTO-1 basis from the quasiexact reference values E^{Ref}. Here MGS denotes the molecular ground state, MS1 and MS2 denote the first and the second excited molecular bound states, respectively, while TS1, TS2, and TS3 denote the trap states. The insets on the right provide a comparison of the energies (a), and energy deviations (b), at $a_s = 0.579\, d_{\mathrm{ho}}$ obtained by the two GTO basis sets, GTO-1 ($N_{\mathrm{GTO}} = 80$, left column) and GTO-2 ($N_{\mathrm{GTO}} = 96$, right column), shifted horizontally with respect to each other for better readability).

B. Energy spectrum

The energies of the ground state and some lower-lying excited states are shown in Fig. 3 as a function of the effective particle-particle interaction. The results were obtained with the largest basis set used in the convergence study in Sec. III A which will be called GTO-1; see Appendix A for details. As is common practice, this interaction strength is expressed in terms of the corresponding *inverse* scattering length a_s that in turn is given in units of the trap length d_{ho}. Recall that small positive (negative) values of d_{ho}/a_s indicate strong repulsive (attractive) interparticle interaction. As already mentioned, in the present calculations the trap length is fixed while the scattering length is varied by tuning the depth of the Morse potential (see Fig. 1).

With the present choice of parameters, the negative values of d_{ho}/a_s correspond to the case where the Morse potential does not support any bound state. In the limit of vanishing attractive interaction ($d_{\mathrm{ho}}/a_s \to -\infty$) the ground-state

energy approaches the one of the lowest-lying trap state, i.e., the ground state of two noninteracting particles in a harmonic-oscillator potential ($3\hbar\omega$). With increasing depth of the Morse potential describing the interparticle interaction (d_{ho}/a_s approaching zero from below) the ground-state energy decreases. As discussed in Appendix B, a further increase of the depth D_e of the Morse potential leads to a Feshbach resonance due to the appearance of a bound state. The scattering length changes from $-\infty$ to $+\infty$ at the resonance and thus its inverse is continuous around $d_{\mathrm{ho}}/a_s = 0$, as is the ground-state energy. The latter decreases further with increasing depth of the Morse potential, since the bound state becomes more strongly bound. The effective interaction between two unbound, colliding atoms in this region is repulsive; however, the repulsion strength decreases with increasing depth of the Morse potential. As the bound state becomes more strongly bound, the influence of the trap potential becomes less important and finally negligible.

Since the relative motion and the center-of-mass motion separate for a harmonic trap, there is an infinite number of states separated by $\hbar\omega$ that correspond to the relative-motion ground state but possess excitations in the center-of-mass motion (see Refs. [14,23,82] for further details). In Fig. 3(a) the four lowest-lying states are shown. These, in the case of positive values of a_s bound molecular states, are denoted as MGS (molecular ground state, no center-of-mass excitation, total angular quantum number $L = 0$), MS1 (one quantum of center-of-mass excitation, $L = 1$), and MS2 (two quanta of center-of-mass excitation, $L = 0$ and $L = 2$). Due to the isotropic harmonic trap potential, the MS2 $L = 0$ and $L = 2$ states are degenerate, but, as a result of the finite basis set, deviations from this degeneracy can be seen, especially for large positive a_s values. In contrast to the exact results (see the results of the reference calculation), the curves of the states MGS, MS1, and MS2 obtained with the GTO basis differ only approximately by a quantum of center-of-mass energy $\hbar\omega$. For $a_s < 0$ the agreement to the reference results is very good and all states converge asymptotically for $d_{\mathrm{ho}}/a_s \to -\infty$ to the corresponding trap states describing noninteracting particles (their energies being indicated by black dashed lines). However, there is a visible increasing deviation from the reference results for increasing positive values of a_s; see the deviations from the reference results shown in Fig. 3(b). Furthermore, the best agreement is achieved for the ground-state MGS. It is similar for the states MS1 $L = 1$ and MS2 $L = 0$, though slightly better for the MS1 state. The largest deviations are observed for the MS2 $L = 2$ state. However, the shape of the deviation curves is very similar for all four states.

Since for the considered depths of the Morse potential at most one molecular bound state is supported, the states with excitation in the relative-motion degree of freedom are all trap states and would be unbound continuum states in the absence of a trap. The lowest-lying trap state (here denoted by TS1) has total angular momentum $L = 0$ and is in the center-of-mass ground state of the harmonic potential, but has two quanta of excitation in the relative motion ($2\hbar\omega$). Therefore, it lies in the limit $d_{\mathrm{ho}}/a_s \to -\infty$ by about the energy difference $\Delta E = 2\hbar\omega$ above the ground state at $E = 5\hbar\omega$. As the molecular bound state emerges for positive a_s and the effective interaction between the atoms decreases, the TS1 state approaches asymptotically for $d_{\mathrm{ho}}/a_s \to +\infty$ the energy of the ground state of two noninteracting atoms in a harmonic potential, i.e., $E = 3\hbar\omega$. A very similar behavior is seen in Fig. 3 for the state named TS2, but the energy curve is shifted by $2\hbar\omega$ compared to the one of TS1, since the two states differ by two quanta of relative-motion excitation. Thus the energies differ exactly by this value for all scattering lengths a_s if a fully converged result is considered. In Fig. 3 the state TS3 is also shown which possesses the total angular-momentum quantum number $L = 2$ and is thus fivefold degenerate. Its energy shows an even smaller dependence on the interatomic interaction than for the states TS1 and TS2. In fact, TS3 is nearly independent of the interatomic interaction. However, a slight deviation is observed for increasing positive values of d_{ho}/a_s. This is due to the fact that in the ultracold regime, the s-wave scattering is typically dominant, as the centrifugal barrier suppresses higher-order partial waves. If the interaction potential is broadened, then the centrifugal barrier is effectively lowered, allowing contributions from channels beyond the s-wave channel [84]. Consequently, the weak deviation of the TS3 state from the horizontal line at $E = 5\hbar\omega$ provides direct evidence of the d-wave interactions.

At first glance, the deviations of the GTO results from the reference ones show a similar qualitative behavior for the trap states and the molecular bound states. The accuracy decreases as the inverse scattering length varies from $-\infty$ to $+\infty$. A slight deviation from the trend is noticed for $L = 0$ (TS1) at $d_{\mathrm{ho}}/a_s = 1.502$ and $L = 1$ (TS2) at $d_{\mathrm{ho}}/a_s = 1.727$. This is due to the fact that there are crossings to higher bound state(s) at these points, lowering the energy of these two trap states (see Ref. [85]). However, compared to the molecular bound states, the decrease of accuracy is less pronounced for the trap states, especially for positive values of the scattering length. Furthermore, the TS3 state shows the smallest deviation from the correct result. This is in accordance with the earlier mentioned expectation that the GTO basis functions are more suitable for describing the trap states, while more efforts (basis functions) are required to properly describe the atom-atom interaction. Therefore, state TS3 with an energy that is almost independent on the interatomic interaction can be most accurately described.

In order to obtain more precise results, the basis set parameters should be optimized separately both for each value of a_s and for each state. While an extensive study of basis set convergence is beyond the scope of this work, it is nevertheless of interest to explore whether and how the basis set could be improved, especially in the regime of positive scattering length values where the molecular state becomes more deeply bound, i.e., when the interatomic interaction is important. Thus for $a_s = 0.579\, d_{\mathrm{ho}}$ ($d_{\mathrm{ho}}/a_s = 1.727$) a second larger basis set named GTO-2 was introduced and optimized for describing the ground state (see Appendix A).

A comparison of the results obtained with GTO-1 and GTO-2 is given in the inset of Fig. 3. Besides state TS3, all energies obtained with GTO-2 are lower than the ones yielded with basis set GTO-1; see Fig. 3(a). In accordance with the empirical experience that a lower energy corresponds to a more accurate result [86], the errors of all but the TS3 state are reduced if GTO-2 is adopted; see Fig. 3(b). The improvement comes at the cost of substantially increased computational

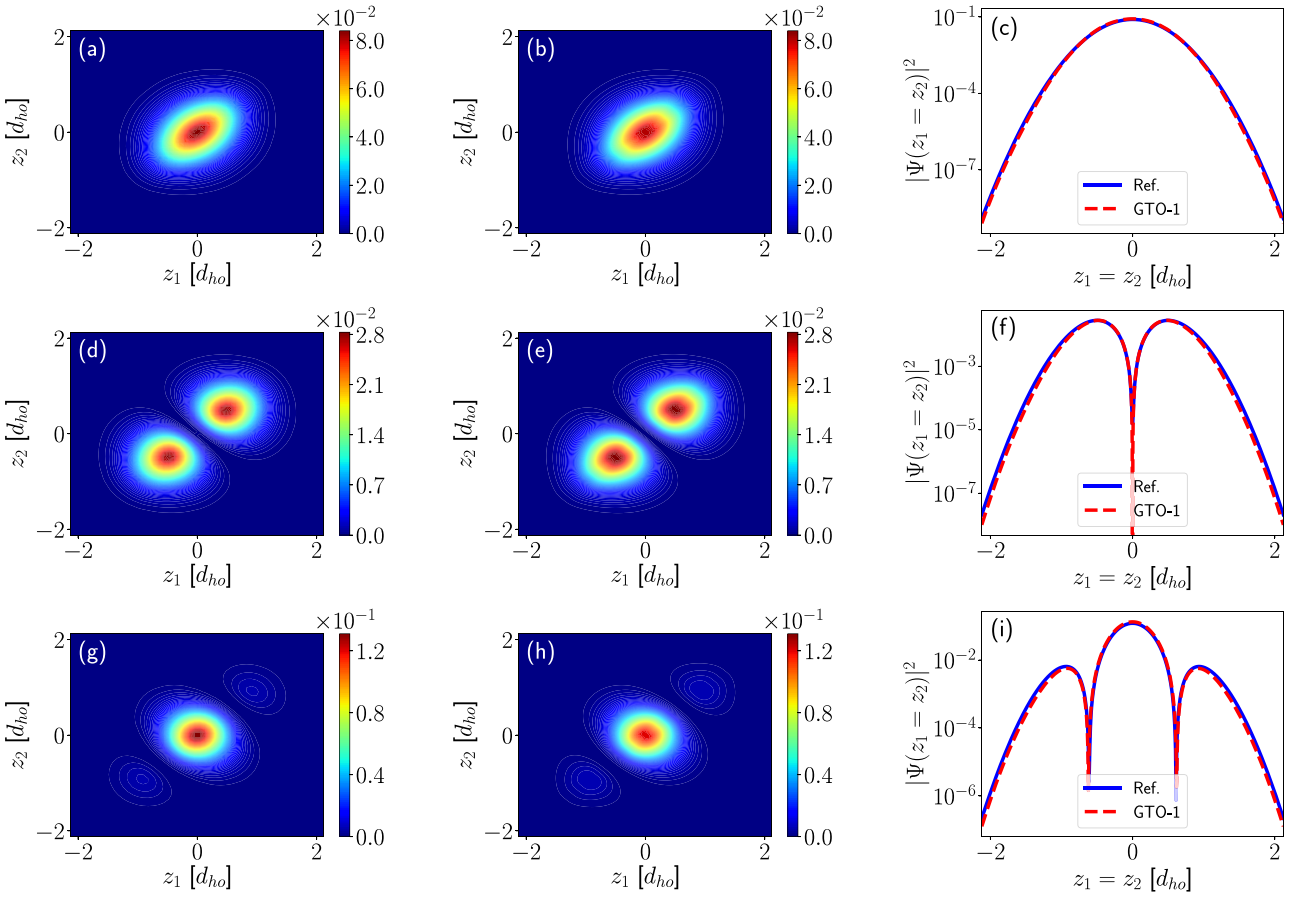


FIG. 4. Cuts through the six-dimensional probability density (squared wave function) along the $[z_1, z_2]$ plane ($|\Psi(z_1, z_2; x_1 = x_2 = y_1 = y_2 = 0)|^2$) for an attractive interaction characterized by $d_{\rm ho}/a_s = -0.392$. [(a)–(c)] MGS state ($L = 0$) (a) GTO-1 basis set ($E^{\rm GTO} = 2.484\,\hbar\omega$), (b) reference result ($E^{\rm Ref} = 2.483\,\hbar\omega$), and (c) one-dimensional cut along the diagonal $z_1 = z_2$ for both GTO-1 basis set and reference. [(d)–(f)] As in (a)–(c) but for the MS1 state ($L = 1$, $E^{\rm GTO} = 3.491\,\hbar\omega$, $E^{\rm Ref} = 3.483\,\hbar\omega$). [(g)–(i)] As in (a)–(c) but for MS2 ($L = 0$, $E^{\rm GTO} = 4.495\,\hbar\omega$, $E^{\rm Ref} = 4.483\,\hbar\omega$).

time, 929 s (GTO-2) compared to 212 s (GTO-1). However, it proves that the energies can be systematically improved if a correspondingly larger basis is adopted. Furthermore, the result highlights the importance of angular correlation for describing (strongly) interacting particles when adopting a CI approach, since it is the GTOs with larger σ values that lead to the improvement. While in the present isotropic example the inclusion of angular correlation adopting Cartesian GTOs with large values of σ is rather inefficient, it should be emphasized that for the intended applications (nonisotropic tweezer arrays) these GTOs are also important for describing the nonisotropic shape of the wave functions.

Since the highly lying TS3 state is only extremely weakly affected by the interatomic interaction, it is not fully unexpected that more GTOs with small value of σ are found to be more important for its description than those with large values of σ. Especially the description of higher-lying trap states requires less compact GTOs with diffuse exponents, while the optimization of the ground-state energy favors more compact GTOs. On the other hand, especially for highly excited states the wave functions possess more and more nodes and thus also require the inclusion of GTOs with larger σ values. Alternatively, additional GTOs that are not centered at the minima of the trap potential could be used.

In conclusion, the results indicate that adopting the new approach reasonable energy spectra can be obtained with relatively small computational efforts. Enlarging the basis set, as well as optimizing the basis-set parameters for a given interatomic interaction potential or state, allows for more accurate energy spectra. The findings are consistent, thus indicating the proper implementation.

C. Eigenfunction analysis

In this section, the six-dimensional eigenfunctions obtained with the present GTO approach are discussed and compared with those produced with the reference approach in relative-motion coordinates based on B splines and spherical harmonics. Figure 4 shows cuts along the $[z_1, z_2]$ plane ($x_1 = x_2 = y_1 = y_2 = 0$) through the probability densities of the MGS, MS1, and MS2 states for an attractive interaction characterized by $d_{\rm ho}/a_s = -0.392$, which corresponds to the potential depth $D_e = 3.0\,\hbar\omega$. Figures 4(a) and 4(b) depict the cuts through the MGS probability (total angular momentum $L = 0$, see Fig. 3), obtained with either the GTO-1 basis set and the reference calculation, respectively. For a more quantitative comparison, Fig. 4(c) shows in addition the one-dimensional cut through the density along the diagonal

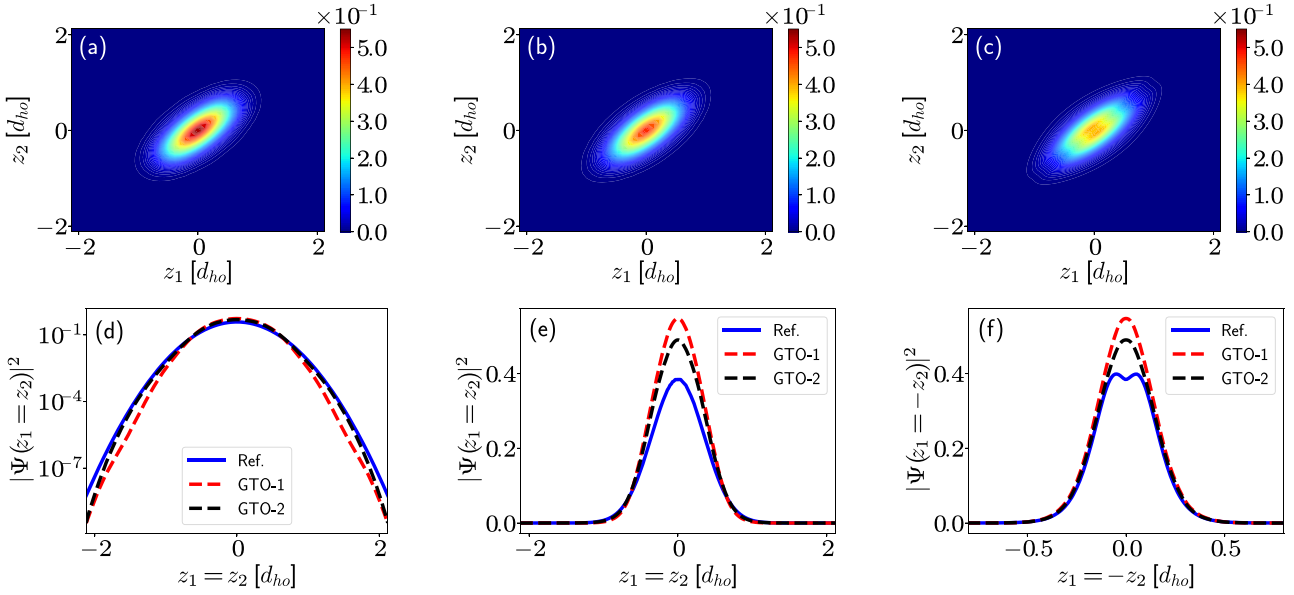


FIG. 5. Same as in Fig. 4 but for a more deeply bound ground-state MGS ($d_{\mathrm{ho}}/a_s = 1.727$). Upper row: (a) GTO-1 basis set ($E = -1.393\,\hbar\omega$), (b) GTO-2 basis set ($E = -1.442\,\hbar\omega$), and (c) reference result ($E = -1.497\,\hbar\omega$). Lower row: One-dimensional cuts through the probability densities, (d) along the diagonal $z_1 = z_2$ (log scale), (e) along the diagonal $z_1 = z_2$ (linear scale), and (f) along the antidiagonal $z_1 = -z_2$ (linear scale).

$z_1 = z_2$. For symmetry reasons, the ground-state MGS is nodeless. Both atoms preferentially stay together in the middle of the trap (maximum at $z_1 = z_2 = 0$). Very good agreement is found for the results obtained either with the GTO approach or the reference calculation.

Figures 4(d) to 4(f) show the corresponding results for the MS1 state ($L = 1$). The two-dimensional cut through the probability density possesses two lobes for $z_1 = z_2 \neq 0$) as well as a nodal plane along the antidiagonal ($z_1 = -z_2$). Consequently, there is a node in the one-dimensional cut at $z_1 = z_2 = 0$. Due to their attractive interaction, the two atoms still stay preferentially together but not in the middle of the trap. The agreement with the reference result is again very good, though slightly worse than for the ground state, as is visible in Fig. 4(f) especially away from the maxima, i.e., for larger absolute values of $z_1 = z_2$. A similar result is obtained for the state MS2 ($L = 0$), whose probability density shows two nodal planes in the two-dimensional cut presented in Figs. 4(g) and 4(h) and two nodes in the one-dimensional cut in Fig. 4(i). (Due to the finite numerical resolution adopted for plotting, the two nodes have a finite value.) While the overall agreement with the quasiexact reference results is still very good, there are already small, but visible differences at the maxima.

As has been discussed in Sec. III B, the accurate description of the states becomes more challenging, if (large) positive values of d_{ho}/a_s and thus repulsive interatomic interaction is considered. For example, the ground-state energy for $d_{\mathrm{ho}}/a_s = 1.727$ was shown to be much closer to the quasiexact reference result, if basis set GTO-2 instead of GTO-1 was adopted, since basis functions with larger σ values (angular momenta) were required for capturing a larger fraction of the angular correlation. In Fig. 5 the earlier introduced two- and one-dimensional probability densities of the ground state (MGS) are shown for basis GTO-1, as well as GTO-2, and compared with the reference results. Already the two-dimensional cuts ($z_1, z_2; x_1 = x_2 = y_1 = y_2 = 0$) show a reasonable agreement but also clearly visible differences. Again, a more quantitative picture is obtained when looking at the one-dimensional cuts along the diagonal ($z_1 = z_2$). While the deviation to the reference result is already visible for the logarithmic plot, it becomes even more evident on the linear scale. In accordance with the improved energy, also the density obtained with GTO-2 compares better with the reference density than the GTO-1 result, but the deviation remains rather pronounced. A more careful look at the two-dimensional densities reveals that the GTO results show a rather smooth function with a single maximum. However, the reference density shows some substructure in the center. In fact, there are two maxima slightly offset from the center. This becomes more transparent in the one-dimensional cut along the antidiagonal ($z_1 = -z_2$) shown in Fig. 5(f). While the reference result shows a small dip in the center, this dip is absent in both, the GTO-1 as well as the GTO-2 densities. Thus even the GTO-2 basis is not capable of reproducing this dip that is a consequence of the interatomic interaction.

It needs to be emphasized that the shown densities are pair correlated (conditional) densities. Similarly to most electronic-structure calculations correlation is also here a relatively small effect and the energy of a state depends mostly on the one-particle density. This explains why the energy, especially for the ground state and $d_{\mathrm{ho}}/a_s = 1.727$ is, especially when using GTO-2, rather well agreeing with the reference result, despite the rather large deviations discussed in the context of Fig. 5.

IV. CONCLUSION AND OUTLOOK

In this work, a new numerical method was developed, implemented, and tested that heads for the study of trapped

few-body systems (indistinguishable Bosons and Fermions or distinguishable particles) beyond the mean-field approximation by means of configuration interaction (exact diagonalization). The approach aims for the description of more than two particles in multicentered trap potentials, especially ultracold atoms in optical tweezer arrays. Cartesian Gaussians in absolute coordinates, well established in electronic-structure calculations, are used as basis functions. The six-dimensional particle-particle integrals were formulated and implemented for a realistic diatomic interaction potential, namely the Morse potential. Since the evaluation of the large number of six-dimensional particle-particle interaction integrals is the bottleneck of structure calculations, some efforts were spent to find an efficient, but nevertheless sufficiently accurate implementation of the integral calculation. In order to validate the proper implementation of the integrals, their accuracy, and the computational speed, a full CI calculation of two particles (Bosons) trapped in an isotropic harmonic trap with variable interparticle interaction strength has been performed, since for this system quasiexact results can be obtained. Furthermore, a first investigation of the suitability of Gaussian basis functions has been performed. This included a rudimentary convergence study, also in order to cross-check the results, as an increased basis set should provide lower ground-state energies according to the variational principle.

The obtained results and their comparison to quasiexact reference data appears consistent, indicating a correct formulation and implementation of the integrals as well as the two-particle full CI calculation. The speed of the integral calculation indicates that larger systems of interest are accessible, especially if the integral calculation is parallelized, possibly on graphics cards, as is planned for the future.

The integrals presented in this work form the heart of a currently developed code that allows for both, mean-field and beyond mean-field calculations describing a variable number of particles (identical or nonidentical Bosons or Fermions) trapped in a multicentered potential of arbitrary geometry. In view of the flexibility of Cartesian Gaussians, even anisotropic interactions, such as dipole-dipole interactions, can possibly be implemented as was done in the reference code already [87,88]. While presently the full CI approach is extended to various ways of selecting configurations, future extensions based on the now existing integral package could be the coupled-cluster or full-CI quantum Monte Carlo methods, as well as multiconfiguration self-consistent-field approaches. In fact, as the master integral is derived for arbitrary functions depending on the interparticle distance, it will be interesting to explore the possible extension to methods that includes correlation more efficiently, like Gaussian geminals, R12, F12, or Jastrow-function methods (see, e.g., Ref. [63] and references therein), without having to resort to the resolution-of-identity approximation.

All these approaches will allow for studies of the influence of confining potentials like optical tweezer arrays on, e.g., atomic clocks, qubits made from neutral atoms, or phenomena like Efimov states. Furthermore, inelastic confinement-induced resonances can be studied for more than two particles.

ACKNOWLEDGMENTS

M.u.R. acknowledges the HEC Overseas Scholarships for Ph.D. in Selected Fields, Phase III, Batch-1, 2020 (57558560) provided in collaboration with the DAAD. M.u.R. and A.S. acknowledge support by Berlin Quantum. This work has been partially supported by the Grants No. PID2021-122711NB-C21 funded by MCIN/AEI/10.13039/501100011033 and No. NSF PHY-2309135 granted to the Kavli Institute for Theoretical Physics (KITP). The authors acknowledge helpful discussions with Robert Moszynski and Michal Lesiuk.

DATA AVAILABILITY

The data that support the findings of this article are not publicly available. The data are available from the authors upon reasonable request.

APPENDIX A: BASIS SET

This Appendix describes some generic symmetry properties of GTOs and the details of the two basis sets used in this work, GTO-1 and GTO-2.

The type of Cartesian GTOs depends on the parameter $\sigma := i + k + m$, where i, k, and m are nonnegative integers [see Eq. (4)]. The single GTO with $\sigma = 0$ corresponds to an s-type orbital ($\ell = 0$) and the three GTOs with $\sigma = 1$ correspond to the p-type orbitals with $\ell = 1$ (p_x, p_y, and p_z). However, there are six Cartesian GTOs for $\sigma = 2$ (10 for $\sigma = 3$, etc.) that can be shown to correspond to five d-type orbitals with a quantum number of angular momentum $\ell = 2$ and one additional s-type orbital with $\ell = 0$ (seven f-type orbitals with $\ell = 3$ and 3 p-type orbitals with $\ell = 1$, etc.). It is common practice to name the Cartesian GTOs according to the value of σ, e.g., the $\sigma = 2$ ones are called d-type GTOs, despite the fact that they contain also an $\ell = 0$ orbital. Removing the linear combinations that correspond to $\sigma \neq \ell$ while keeping the remaining linear combinations as basis functions that correspond to $\sigma = \ell$ and a well-defined magnetic quantum number m_ℓ leads to the so-called spherical GTO basis sets. Since the algorithms for evaluating the Hamiltonian matrix elements between basis functions are based on Cartesian GTOs, the use of spherical GTOs involving the corresponding transformations is computationally costly.

In this work, the two Cartesian GTOs basis sets employed are as follows. The first basis set GTO-1 comprises $\sigma = 0$, 1, 2, and 3. Specifically, 4 GTOs for each corresponding orbital type (e.g., s, p_x, p_y, p_z, etc.) are adopted. This yields 4 GTOs for $\sigma = 0$, 12 GTOs for $\sigma = 1$, 24 GTOs for $\sigma = 2$, and 40 GTOs for $\sigma = 3$, adding to a total number of $N_{\mathrm{GTO}} = 80$ functions. For simplicity, the same four values of the exponents $\tau = 0.3$, 0.5, 1.0 and 2.2 in Eq. (4) are adopted, independently of σ (see the discussion in Sec. III A for details). With $N_{\mathrm{GTO}} = 80$ and no use of symmetry, $N_{\mathrm{CF}} = 3240$ configurations Φ are obtained which is, thus, the dimension of the CI matrix. The second basis set is named GTO-2. In this basis set for $\sigma = 0$, 1, 2, and 3 only 3 GTOs for each orbital type (e.g., s, p_x, p_y, p_z, etc.) are used, with the corresponding exponents $\tau = 1.0$, 1.7, and 2.3. Additionally, GTO-2 contains GTOs with $\sigma = 4$ and 5 (g- and h-type orbitals) with

only one exponent $\tau = 1.0$ for each orbital type, resulting in a total of $N_{\mathrm{GTO}} = 96$ functions and 4656 configurations.

Since the configurations are directly expanded in (nonorthogonal) GTOs, a generalized eigenvalue problem needs to be solved. For validation purposes, two different LAPACK diagonalization routines, DSYGV and DSYEV, are employed. The results obtained from both routines are found to be in perfect agreement for the leading 12 digits.

In the reference calculations, we used 52 B splines for both relative and center-of-mass computations, with maximum values of angular momentum $\ell_{\max} = 6$ and the magnetic number $|m_{\ell,\max}| = 6$ for the spherical harmonics (see Refs. [14,23,82] for further details on the reference approach).

APPENDIX B: SCATTERING LENGTH

This Appendix describes the procedure used to compute and vary the scattering length. It also summarizes the underlying physical assumptions and parameter choices.

Experimentally, the interactions between ultracold atoms can be almost arbitrarily tuned with the help of magnetic Feshbach resonances [8,9,89,90]. Furthermore, due to the low temperatures the effective interactions among Bosons are dominated by s-wave scattering and can be characterized by a single parameter, i.e., the s-wave scattering length (a_s) [83]. In this work, the s-wave scattering length is tuned by a variation of the depth of the Morse potential D_e while keeping $R_m = 0.212\, d_{\mathrm{ho}}$ and $a_m = \sqrt{20}\, d_{\mathrm{ho}}^{-1}$ constant. The scattering length as a function of the variation of the Morse potential depth is shown in Fig. 1. The regions of negative and positive scattering lengths correspond to an effectively attractive or repulsive interaction between the two atoms, respectively. Note that at the poles (orange dash-dotted lines) occurring for $D_e = [3.823,\ 24.877,\ 65.075]\,\hbar\omega$, the scattering length diverges, changing from infinitely strong attraction ($a_s \to -\infty$) to infinitely strong repulsion ($a_s \to +\infty$). These poles mark the positions of the Feshbach resonances where an additional molecular bound state appears, since the number of molecular bound states that are supported increases with the depth of the particle-interaction potential. In the calculations performed in this work, the range $D_e \in [0.5 - 15.0\,]\,\hbar\omega$ (gray and light blue shaded areas) is considered. Within the gray region, the Morse potential is too shallow to support any bound state. However, the first bound state appears in the area marked by the light blue color.

[1] B. M. Spar, E. Guardado-Sanchez, S. Chi, Z. Z. Yan, and W. S. Bakr, Phys. Rev. Lett. **128**, 223202 (2022).

[2] L. Pause, T. Preuschoff, D. Schäffner, M. Schlosser, and G. Birkl, Phys. Rev. Res. **5**, L032009 (2023).

[3] D. Bloch, B. Hofer, S. R. Cohen, A. Browaeys, and I. Ferrier-Barbut, Phys. Rev. Lett. **131**, 203401 (2023).

[4] H. Levine, A. Keesling, G. Semeghini, A. Omran, T. T. Wang, S. Ebadi, H. Bernien, M. Greiner, V. Vuletić, H. Pichler *et al.*, Phys. Rev. Lett. **123**, 170503 (2019).

[5] A. W. Young, W. J. Eckner, W. R. Milner, D. Kedar, M. A. Norcia, E. Oelker, N. Schine, J. Ye, and A. M. Kaufman, Nature (London) **588**, 408 (2020).

[6] A. M. Kaufman and K.-K. Ni, Nat. Phys. **17**, 1324 (2021).

[7] Y. Yu, K. Wang, J. D. Hood, L. R. B. Picard, J. T. Zhang, W. B. Cairncross, J. M. Hutson, R. Gonzalez-Ferez, T. Rosenband, and K.-K. Ni, Phys. Rev. X **11**, 031061 (2021).

[8] C. Chin, R. Grimm, P. Julienne, and E. Tiesinga, Rev. Mod. Phys. **82**, 1225 (2010).

[9] M. Aymar, J. Phys. B **11**, 1413 (1978).

[10] C. Ti, Y. Shen, M.-T. Ho Thanh, Q. Wen, and Y. Liu, Sci. Rep. **10**, 20099 (2020).

[11] D. K. Ruttley, A. Guttridge, S. Spence, R. C. Bird, C. R. Le Sueur, J. M. Hutson, and S. L. Cornish, Phys. Rev. Lett. **130**, 223401 (2023).

[12] D. K. Ruttley, A. Guttridge, T. R. Hepworth, and S. L. Cornish, PRX Quantum **5**, 020333 (2024).

[13] P.-I. Schneider, S. Grishkevich, and A. Saenz, Phys. Rev. A **80**, 013404 (2009).

[14] D. Capecchi, C. Cantillano, M. J. Mark, F. Meinert, A. Schindewolf, M. Landini, A. Saenz, F. Revuelta, and H.-C. Nägerl, Phys. Rev. Lett. **131**, 213002 (2023).

[15] G. Bougas, S. I. Mistakidis, P. Giannakeas, and P. Schmelcher, Phys. Rev. A **106**, 043323 (2022).

[16] G. Bougas, S. I. Mistakidis, and P. Schmelcher, Phys. Rev. A **100**, 053602 (2019).

[17] G. Bougas, S. Mistakidis, P. Giannakeas, and P. Schmelcher, New J. Phys. **23**, 093022 (2021).

[18] S. Sala, P.-I. Schneider, and A. Saenz, Phys. Rev. Lett. **109**, 073201 (2012).

[19] E. Haller, M. J. Mark, R. Hart, J. G. Danzl, L. Reichsöllner, V. Melezhik, P. Schmelcher, and H.-C. Nägerl, Phys. Rev. Lett. **104**, 153203 (2010).

[20] M. Valiente and K. Mølmer, Phys. Rev. A **84**, 053628 (2011).

[21] V. S. Melezhik and P. Schmelcher, Phys. Rev. A **84**, 042712 (2011).

[22] S. Sala, G. Zürn, T. Lompe, A. N. Wenz, S. Murmann, F. Serwane, S. Jochim, and A. Saenz, Phys. Rev. Lett. **110**, 203202 (2013).

[23] S. Sala and A. Saenz, Phys. Rev. A **94**, 022713 (2016).

[24] V. N. Efimov, Sov. J. Nucl. Phys. **12**, 589 (1971) [Yad. Fiz. **12**, 1080 (1970)].

[25] V. N. Efimov, Phys. Lett. B **33**, 563 (1970).

[26] B. D. Esry, C. H. Greene, and J. P. Burke, Phys. Rev. Lett. **83**, 1751 (1999).

[27] F. Werner and Y. Castin, Phys. Rev. Lett. **97**, 150401 (2006).

[28] F. Ferlaino, S. Knoop, M. Berninger, W. Harm, J. P. D'Incao, H.-C. Nägerl, and R. Grimm, Phys. Rev. Lett. **102**, 140401 (2009).

[29] P. Naidon and S. Endo, Rep. Prog. Phys. **80**, 056001 (2017).

[30] M. D. Higgins and C. H. Greene, Phys. Rev. A **106**, 023304 (2022).

[31] G. Bougas, S. I. Mistakidis, P. Schmelcher, C. H. Greene, and P. Giannakeas, Phys. Rev. Res. **5**, 043134 (2023).

[32] J. R. Armstrong, N. T. Zinner, D. V. Fedorov, and A. S. Jensen, J. Phys. B **44**, 055303 (2011).

[33] X. Y. Yin, D. Blume, P. R. Johnson, and E. Tiesinga, Phys. Rev. A **90**, 043631 (2014).

[34] P. Jeszenszki, A. Y. Cherny, and J. Brand, Phys. Rev. A **97**, 042708 (2018).

[35] P. Jeszenszki, A. Alavi, and J. Brand, Phys. Rev. A **99**, 033608 (2019).

[36] S. F. Boys, Proc. R. Soc. Lond. A **200**, 542 (1950).

[37] D. Rakshit and D. Blume, Phys. Rev. A **86**, 062513 (2012).

[38] G. M. Barca and P.-F. Loos, J. Chem. Phys. **147**, 024103 (2017).

[39] B. D. Esry and C. H. Greene, Phys. Rev. A **60**, 1451 (1999).

[40] F. Brauneis, H.-W. Hammer, S. M. Reimann, and A. G. Volosniev, Phys. Rev. A **111**, 013303 (2025).

[41] In fact, already within the mean-field description, the standard δ pseudopotential employing the trap-free scattering length does not lead to an accurate description. Instead, an energy-dependent scattering length [91] is usually adopted that is, however, only available after a full treatment of the correct interparticle interaction *together* with the confining trap potential.

[42] S. Sala, J. Förster, and A. Saenz, Phys. Rev. A **95**, 011403(R) (2017).

[43] J. M. Deutsch, Phys. Rev. A **43**, 2046 (1991).

[44] M. Srednicki, Phys. Rev. E **50**, 888 (1994).

[45] N. Shiraishi and K. Matsumoto, Nat. Commun. **12**, 5084 (2021).

[46] S. Moudgalya, N. Regnault, and B. A. Bernevig, Phys. Rev. B **98**, 235156 (2018).

[47] C. J. Turner, A. A. Michailidis, D. A. Abanin, M. Serbyn, and Z. Papić, Nat. Phys. **14**, 745 (2018).

[48] M. Serbyn, D. A. Abanin, and Z. Papić, Nat. Phys. **17**, 675 (2021).

[49] F. Revuelta, E. G. Vergini, R. M. Benito, and F. Borondo, Phys. Rev. E **85**, 026214 (2012).

[50] R. J. Bartlett and M. Musiał, Rev. Mod. Phys. **79**, 291 (2007).

[51] L. Cao, S. Krönke, O. Vendrell, and P. Schmelcher, J. Chem. Phys. **139**, 134103 (2013).

[52] K. M. Daily and D. Blume, Phys. Rev. A **81**, 053615 (2010).

[53] J. Rotureau, I. Stetcu, B. R. Barrett, M. C. Birse, and U. van Kolck, Phys. Rev. A **82**, 032711 (2010).

[54] C. H. Greene, P. Giannakeas, and J. Pérez-Ríos, Rev. Mod. Phys. **89**, 035006 (2017).

[55] E. Hiyama and M. Kamimura, Front. Phys. **13**, 132106 (2018).

[56] D. Blume, Rep. Prog. Phys. **75**, 046401 (2012).

[57] J. von Stecher and C. H. Greene, Phys. Rev. A **80**, 022504 (2009).

[58] M. W. C. Sze, A. G. Sykes, D. Blume, and J. L. Bohn, Phys. Rev. A **97**, 033608 (2018).

[59] M. Silkowski, M. Lesiuk, and R. Moszynski, J. Chem. Phys. **142**, 124102 (2015).

[60] J. G. Balcerzak, M. Lesiuk, and R. Moszynski, Phys. Rev. A **96**, 052510 (2017).

[61] S. Grishkevich and A. Saenz, Phys. Rev. A **80**, 013403 (2009).

[62] A. Szabo and N. S. Ostlund, *Modern Quantum Chemistry: Introduction to Advanced Electronic Structure Theory* (Courier Corporation, Garden City, NY, 1996).

[63] A. Grüneis, S. Hirata, Y.-y. Ohnishi, and S. Ten-No, J. Chem. Phys. **146**, 080901 (2017).

[64] D. Casanova, WIREs Comput. Mol. Sci. **12**, e1561 (2022).

[65] H.-J. Werner and P. J. Knowles, J. Chem. Phys. **89**, 5803 (1988).

[66] G. H. Booth, A. J. Thom, and A. Alavi, J. Chem. Phys. **131**, 054106 (2009).

[67] N. M. Tubman, J. Lee, T. Y. Takeshita, M. Head-Gordon, and K. B. Whaley, J. Chem. Phys. **145**, 044112 (2016).

[68] B. O. Roos, *The Multiconfigurational (MC) Self-consistent Field (SCF) Theory* (Springer, Berlin, 1992).

[69] P. Å. Malmqvist, A. Rendell, and B. O. Roos, J. Phys. Chem. **94**, 5477 (1990).

[70] J. Olsen, Int. J. Quantum Chem. **111**, 3267 (2011).

[71] B. O. Roos, P. R. Taylor, and P. E. Sigbahn, Chem. Phys. **48**, 157 (1980).

[72] P.-I. Schneider, S. Grishkevich, and A. Saenz, Phys. Rev. A **87**, 053413 (2013).

[73] G. Herzberg, *Molecular Spectra and Molecular Structure. Spectra of Diatomic Molecules* (Van Nostrand Reinhold, New York, 1950), Vol. 1.

[74] P. Morse, Phys. Rev. **34**, 57 (1929).

[75] R. A. Buckingham, Proc. R. Soc. Lond. A **168**, 264 (1938).

[76] L. E. McMurchie and E. R. Davidson, J. Comput. Phys. **26**, 218 (1978).

[77] Note that there are typos in the Eqs. (11) and (12) of Ref. [60]. In both equations the term E_u^{mn} should be E_v^{mn}. Likewise, in Eq. (12) the term $E_{u'}^{m'n'}$ should be $E_{v'}^{m'n'}$.

[78] C. C. M. Samson, W. Klopper, and T. Helgaker, Comput. Phys. Commun. **149**, 1 (2002).

[79] E. W. Hobson, *The Theory of Spherical and Ellipsoidal Harmonics* (Chelsea, New York, 1965).

[80] H. B. Schlegel and M. J. Frisch, Int. J. Quantum Chem. **54**, 83 (1995).

[81] Here a factor of 2 was missing in Eq. (45) of Ref. [59], which was subsequently corrected in Eq. (25) of Ref. [60].

[82] S. Grishkevich, S. Sala, and A. Saenz, Phys. Rev. A **84**, 062710 (2011).

[83] J. Weiner, V. S. Bagnato, S. Zilio, and P. S. Julienne, Rev. Mod. Phys. **71**, 1 (1999).

[84] S. Sala, Ph.D. thesis, Humboldt-Universität zu Berlin, Germany, 2016.

[85] At these points the GTOs energies are lowered due to an avoided crossing with higher bound state(s) of the same symmetry, which are not shown in the graph. This lower energy accidentally leads to a better agreement with the quasiexact results.

[86] The variational principle only applies to the lowest state of each symmetry. For excited states it applies strictly only, if the state is orthogonal to all lower-lying *exact* states.

[87] B. Schulz, S. Sala, and A. Saenz, New J. Phys. **17**, 065002 (2015).

[88] B. Schulz and A. Saenz, ChemPhysChem **17**, 3747 (2016).

[89] T. Loftus, C. A. Regal, C. Ticknor, J. L. Bohn, and D. S. Jin, Phys. Rev. Lett. **88**, 173201 (2002).

[90] S. Grishkevich, P.-I. Schneider, Y. V. Vanne, and A. Saenz, Phys. Rev. A **81**, 022719 (2010).

[91] D. Blume and C. H. Greene, Phys. Rev. A **65**, 043613 (2002).